Full Paper

Tracking Dynamic Source Direction with a Novel Stationary Electronic Nose System

Jie Cai [1,]***and David C. Levy** [2,]*****

Building J03, School of Electrical and Information Engineering, Faculty of Engineering, University of Sydney, NSW 2006, Australia

* Authors to whom correspondence should be addressed; E-mails: jcai@ee.usyd.edu.au (Jie Cai), dlevy@ee.usyd.edu.au (David C. Levy)

Abstract: Arrays of chemical sensors, usually called electronic noses (ENose), are widely used in industry for classifying and identifying odours. They may also be used to locate the position and detect the direction of an emission source. Usually this task is performed by an ENose cooperating with a mobile vehicle, but when a source is instantaneous, or the surrounding terrain is hard for vehicles to traverse, an alternative approach is needed. Thus a three-step method for a stationary ENose with a novel structure to detect the direction of a dynamic source is presented in this paper. The method uses the ratio of measured concentration from different sensors (C_n / C_1 where n=2, 4) as a discriminator. In addition, this method could easily be adapted to robotics as an optimized algorithm for path tracking to a source location. The paper presents the results of a simulation of the method.

Keywords: Electronic nose, Direction detection, Dynamic source tracking, Nature wind situation

1. Introduction

Today quality control with electronic noses is widely used in the food and beverage industry. The classification and identification of chemical emissions or aromas using ENoses is also applied in pollution control and fire detection [1-8]. The techniques to support those applications, such as feature extraction and pattern recognition, are very well developed [9-15]. Based on the application of these techniques, information such as concentration is derived. The concentrations derived from several ENoses are used to locate the position or detect the direction of an aroma source. Using well

developed robotics techniques this task is normally performed by "mobile sensors", where one or more ENoses is mounted on an autonomous vehicle [16-18]. Such mobile sensors function well when the emission source is not instantaneous and where the outside environment allows the vehicle to reach the source position, even in a dynamic source situation [18]. Mobile sensors, however, face difficulties in solving the problem of an instantaneous source, where the source delivers a short burst of aroma, and complex landscapes which the vehicle cannot negotiate. Thus the requirement arises for locating and detecting a source using stationary sensors.

There are few publications about source localization and detection with stationary sensors. In 2005, Jorg Matthes developed a discrete model method to solve this problem with a spatially distributed network of electronic noses, using more than four ENoses in diffusion and advection situations [19]. Matthes, however, did not consider crosswinds or dynamic sources. In addition, there is a space limitation within Matthes's structure, which does not allow any obstructions among the spatially distributed ENoses. Moreover, it is more expensive to construct such an electronic nose network than a simple ENose system.

In this paper, a method of stationary sensors to detect the direction of both static and dynamic chemical emission sources within natural wind surroundings is presented. The method covers three cases: advection, crosswinds and breaks in the wind. Advection is the case where the wind direction is along the axis of the ENose system (x axis). The crosswind case is considered as advection and y-axis wind effects simultaneously. The case of a break in the wind will be discussed in more detail below.

The whole ENose system is introduced in section II. A new approach for direction detection is presented in section III, which will be divided into the three aspects of: (1) determining the direction of the source in the advection case; (2) resolving the direction in a crosswind and (3) dealing with a break in the wind. A method of tracking dynamic source directions will be presented in section IV. Simulation results are presented in section V; finally some conclusions are drawn in section VI.

2. System Structure

The novel electronic nose system is built with four identical sensors (FIGARO TGS 2610) which are separated by a square impermeable separator with four wings. The sensors and separator will be build on a PCB board. The choice of sensor depends on the gas that is to be detected. For the TGS 2610, odor source could be LP gas. The structure of the system is shown in Figure 1.

The left part is the physical structure of this system. Crosswind vector ($V_{CrossWind}$) could be presented as the sum of x direction vector (V_x) and y direction vector (V_y). The direction of a crosswind is the included angle of the cross wind vector and the axis of the ENose, which is denoted by α. The shape of the sensors is considered as a circle with radius 0.5cm. The dimensions of the separators are 2cm X 2cm for square and each wing has an included angle 45^0 with length $2\sqrt{2}$. The height of separator and wings is 20cm which is much greater than the height of sensor, 1.1 cm. To reduce the dimensions of the system, we assume that the source is a dot source placed on an impermeable surface at the same height as the ENose, ie at z=0, at an unknown position x, y relative to the ENose. Angle θ presents the included angle of the axis of the ENose system and a line connecting the source and the center of the ENose system. This is called the direction of the source.
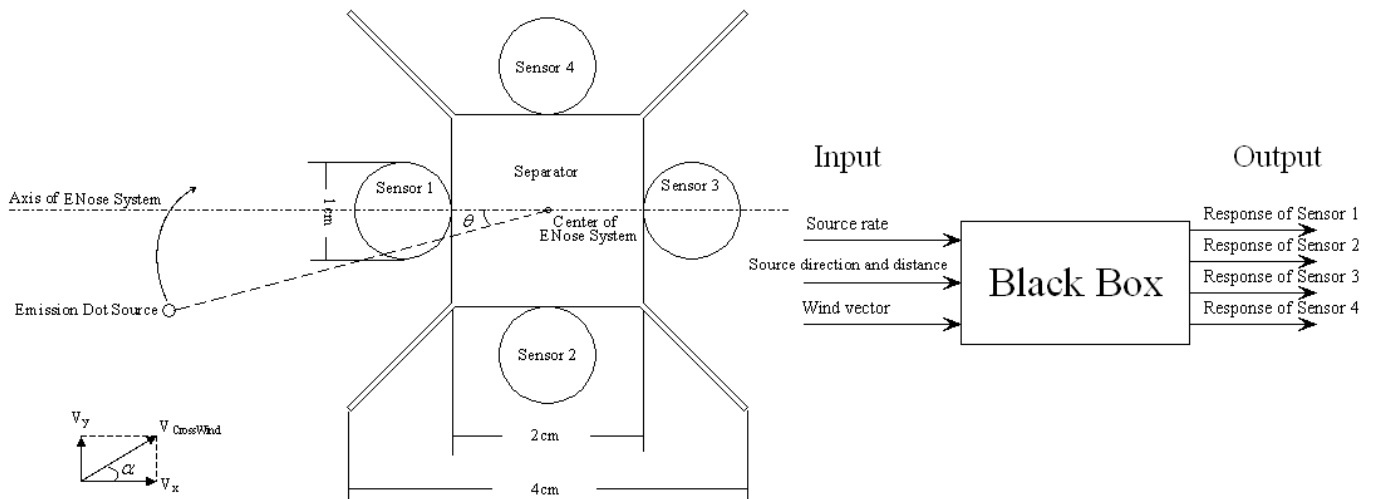
Figure 1. Electronic nose system structure, left part is the physical structure of electronic nose, which contains 4 sensors separated by an impermeable four wings separator; the right part is the black box problem schema for the whole system.

As shown in the right part of Figure 1, this system could be treated as an inverse black box problem, which has unknown input: source direction θ and distance d, source rate and known input wind speed vectors ($V_{CrossWind}$ and α), the output is the measured concentrations from the four sensors, also called the responses of the sensors, denoted by C_j (j=1, 2, 3, 4). In this inverse black box problem we wish to find out the relationship between input and output and then we can inversely solve this problem. It should be noted that in this paper, the source emission strength and its distance (d) are not considered and can be easily avoided in solving for θ, as is discussed in section 3.1.

3. Three-Step Approach to Determine Static Source Direction

In this section, the method to determine the static source direction is given for the two different cases, advection and crosswind. The solution for the source direction angle θ is given in both cases. The case of a break in the wind is discussed at the end of this section. The state of the wind is represented by 2 variables: wind direction α (see Figure 1) and time t. η indicates an angle of the wind off of the x-axis, determined by the accuracy of the real sensors.

If $\alpha <= \eta$, the case is treated as advection;

If $\alpha > \eta$, it is treated as a crosswind;

If

$$V_{wind}(t) = 0, \quad t_1 < t < t_2$$

$$V_{wind}(t) = a, \quad t < t_1 \quad OR \quad t > t_2, \quad \text{where a is a non - zero constant,}$$

it is a break in the wind.

3.1. Determine the direction of source to center of ENose system in advection case

A series of simulations was done to analyse the relation between the source direction angle θ and the sensors responses in the advection case. The simulation is based on the following: (1) make the center point of ENose system the origin, (2) set the x wind speed to 5m/s, the y direction wind speed 0, and the source concentration 10×10^2 ppm, (3) keeping the distance ($d = 1.6$ m) between source and ENose system unchanged, then move the source around the circle of radius d to change the source direction angle θ, (4) record the measured concentration of the four sensors corresponding to angle θ and set the distributed concentration to 0 for next record (C(x, y)=0 for any x and y). Figure 2 shows the relations between angle θ and the simulated series of stable sensors responses.
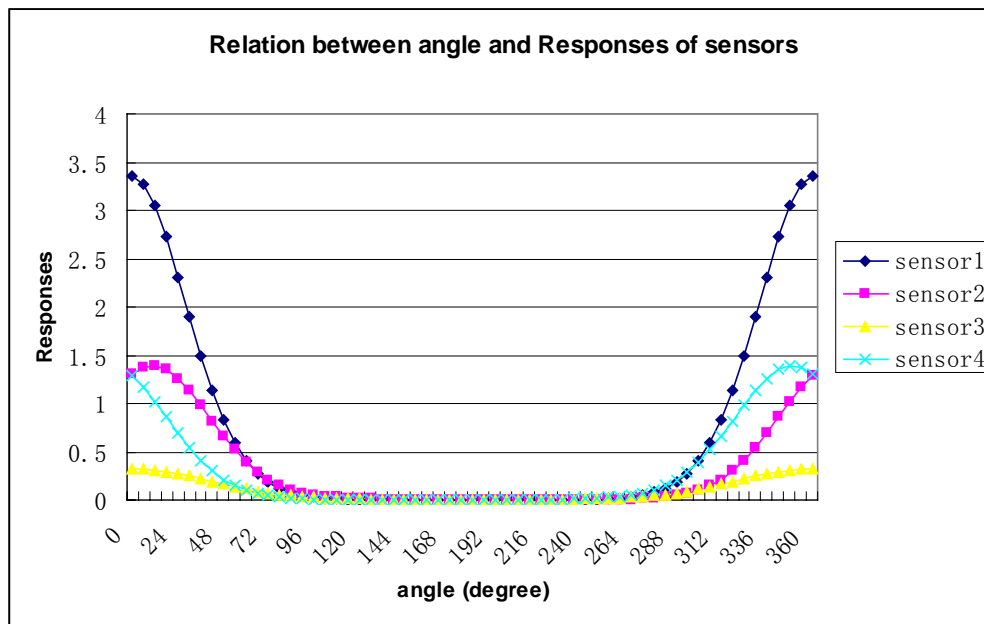
Figure 2. Simulated series of stable sensors responses in advection case for different source directions θ.

In Figure 2, sensor 1 has the highest simulated steady response. The steady response of sensor 2 and 4 are identical about the axis of symmetry, 180^0. The steady response of sensor 3 is ignored. Moreover, from Figure 2 we see the simulated steady responses of the sensors are a periodic function of angle with period of 2π. The simulation result shown in Figure 2 does not depend on the odor used. Any kinds of isotropic diffused odor will have the same simulated result when the simulation is set up as stated in the previous paragraph.

Moreover, for most kinds of sensor, the response will monotonically change with concentration. We use the stable response in our analysis. Thus, when the concentration is stable, the response of sensor will be stable too. Therefore, Figure 2 shows a generic relation between simulated series of stable sensor responses and different source directions.

Now we need to discuss the influence of initial source rate and distance (d) to the concentration, then find a discriminant to determine the source direction. Consider the diffusion equation in advection situation given by [19]
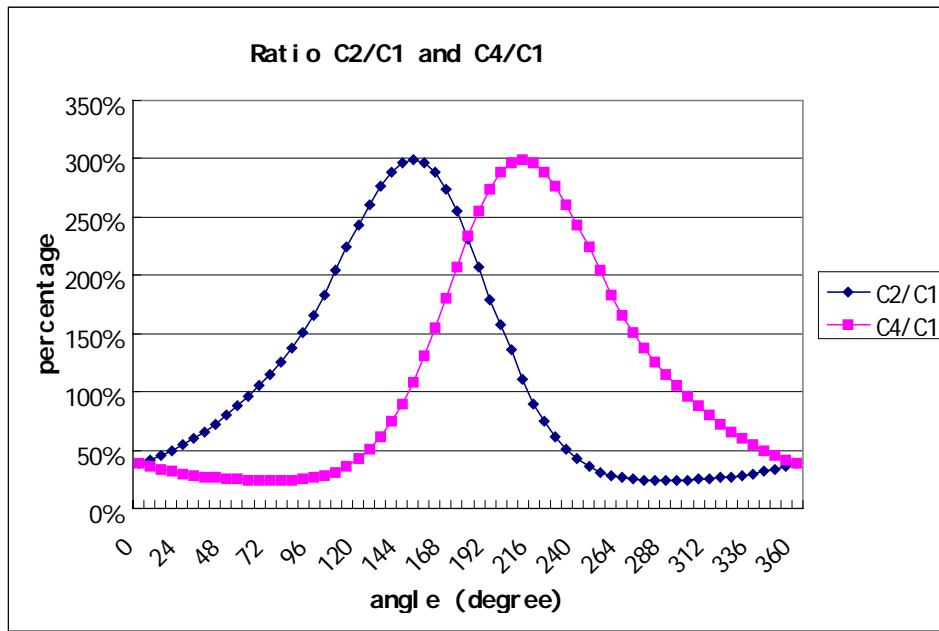
Figure 3. Ratio $\frac{C_2}{C_1}$ and $\frac{C_4}{C_1}$, discriminant of source direction.

$$\frac{\partial C}{\partial t} - D(\frac{\partial^2 C}{\partial x^2} + \frac{\partial^2 C}{\partial y^2} + \frac{\partial^{2C}}{\partial z^2}) + V_x \frac{\partial C}{\partial x}$$

$$= 2q_0 \cdot 1(t-t_0) \cdot \delta(x-x_0) \cdot \delta(y-y_0) \cdot \delta(z-z_0)$$

(1)

where D is diffusion coefficient, q_0 is initial source rate, x y and z is spatial variables. To solve equation (1) at conditions: $C(P,t) \equiv 0$ for t<t$_0$ and for all P(x,y), let $P_0(x_0, y_0)$ denote for the source location, we can solve for large time $t(t \rightarrow \infty)$, and a steady concentration profile as is given in [19]:

$$C(x, \infty, x_0, q_0) = \frac{q_0 \cdot \exp(-\frac{v_x}{2D}(d-(x-x_0)))}{2\pi D d}$$

(2)

Where d is the distance from a certain point P(x,y) to the source location $P_0(x_0, y_0)$.

Corresponding to equation (2), we can see that source rate q_0 will not affect the ratio $\frac{C_n}{C_1}$ (n=2, 4). The distances d_i for four sensors are treated as the same spatially, because the dimension of the ENose system is in centimeters, where the distance d_i usually is in meters. Thus, distance d_i will not affect the ratio $\frac{C_n}{C_1}$ (n=2, 4). Therefore we use ratio $\frac{C_n}{C_1}$ as our discriminant of angle.

Figure 3 shows the ratios, C_2/C_1 and C_4/C_1. It generated from the simulated data of Figure 2. It is difficult for us to separate the sensor responses when the source direction is between 100^0 and 300^0 in Figure 2, but Figure 3 shows us clearly the relationship of the sensors' response between 100^0 and 300^0. We find that C_2/C_1 and C_4/C_1 are symmetrical about the 180^0 axis, and a curve can be fitted using the Matlab curvefit toolbox as shown in Figure 3. The fitted equation is presented in Gauss equation format:

$$\frac{C_2}{C_1} = f(\theta) = 2.061 \cdot e^{-\left(\frac{\theta-154}{51.63}\right)^2} + 1.095 \cdot e^{-\left(\frac{\theta-107.9}{101.7}\right)^2} + 0.6291 \cdot e^{-\left(\frac{\theta-501.5}{191.2}\right)^2} \tag{3}$$

Thus, the angle θ is determined by calculating C_2/C_1, then if the measured concentration of sensor 4 is smaller than sensor 2 according to Figure 1, θ would lie between 0° and 180°, otherwise, θ would between 180° and 360°.

$$\theta = f^{-1}(\theta) \tag{4}$$

Equation (4) is the function to calculate angle θ, which is easily implemented.

3.2. Crosswind case direction detection

In this case, a crosswind with V_x and V_y is applied. We randomly picked a set of wind speeds for V_x and V_y, of 5m/s and 3m/s respectively. A series of simulations was done to analyse this case. Figure 4 shows the relations between angle and the simulated steady sensors' responses in the crosswind case.
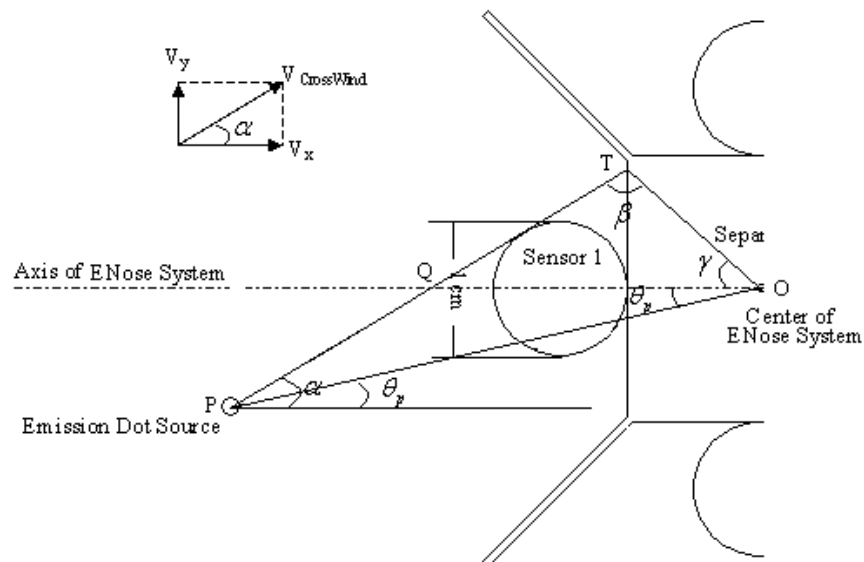
Figure 4. Simulated series of stable sensors responses in crosswind case according to different source direction θ

The diffusion equation in crosswind situation is present as follows:

$$\frac{\partial C}{\partial t} - D\left(\frac{\partial^2 C}{\partial x^2} + \frac{\partial^2 C}{\partial y^2} + \frac{\partial^{2C}}{\partial z^2}\right) + V_x \frac{\partial C}{\partial x} + V_y \frac{\partial C}{\partial y}$$
$$= 2q_0 \cdot 1(t - t_0) \cdot \delta(x - x_0) \cdot \delta(y - y_0) \cdot \delta(z - z_0) \tag{5}$$

We use α to represent the direction of crosswind. Then, rotating the Cartesian coordinate system with the angle α, the new coordinates should be:

$$x' = d \cdot Cos\left(\pi + \tan^{-1}\frac{y}{x} - \alpha\right)$$

$$y' = d \cdot Sin\left(\pi + \tan^{-1}\frac{y}{x} - \alpha\right) \tag{6}$$

where d is the distance between any point P(x,y) and origin O, x' and y' denotes the transferred coordinates, x and y presents the coordinates before transform.

The diffusion equation for the crosswind situation may then be presented as shown in equation (7) with the same conditions as equation (2):

$$C(x, \infty, x_0, q_0) = \frac{q_0 \cdot \exp(-\frac{v_{Crosswind}}{2D}(d - (x' - x'_0)))}{2\pi D d} \tag{7}$$

where $V_{CrossWind} = V_x + V_y$. We can see that Equation (7) is the same as equation (2). As a result, after the coordinate transfer, the analysis for the influence of initial source ratio q_0 and distance d in section 3.1 can be used for the crosswind case. Therefore, ratio $\frac{C_n}{C_1}$ (n=2, 4) is used as a general discriminant for both cases.

Once again, we did the calculation of the ratio C_{2cross}/C_{1cross} and C_{4cross}/C_{1cross}. Fortunately, we found that they have a similar pattern to the Gaussian distribution shown in Figure 3. The ratio for sensor 2 and sensor 4 is symmetrical about axis $\theta = 180^0$. The solid line in Figure 6 presents the ratio C_{2cross}/C_{1cross} in the crosswind case.

Corresponding to Figure 4, we see that the highest simulated series of stable responses belongs to sensor 1. But unlike the responses of sensor 1 in Figure 2, the peak point for sensor 1 in Figure 4 is not reached at 0^0. We will use the peak point angle θ_p to help us find out the relation between ratio C_{2cross}/C_{1cross} and C_2/C_1. We can then calculate the direction angle corresponding to the peak point in Figure 4 for the crosswind case.

After we calculated the peak point for several cases (with different wind directions and source directions) based on the simulation results, we found that the peak point occurs when the following conditions are all satisfied:

  (1) The source position is on a line with slope of crosswind direction α
  (2) This line is a tangent of sensor 1.

The equation for this line is easily given by following equation:

$$-\sqrt{\frac{1}{1 + \tan^2 \alpha}} \cdot x + \tan \alpha \sqrt{\frac{1}{1 + \tan^2 \alpha}} \cdot y = R \tag{8}$$

where R is the radius of sensor 1.

Figure 5 shows the diagram for calculating the peak point angle. $\overline{PT}$ is the tangent with crosswind direction of sensor 1, which may be calculated using equation (8); P is the proposed source position; O is the center of ENose system (origin); T is the intersection point of straight line $\overline{PT}$ and the edge of the separator, Q is the intersection point of $\overline{PT}$ and x axis.

$\overline{TO}$, $\overline{OQ}$, $\overline{QT}$ is known by simply calculating the Euclidean distance using equation (9)

$$d_{X_x X_2} = \left\| X_1 - X_2 \right\|_2 \tag{9}$$

here X_1 and X_2 can be replaced by the point sets {T,O}, {O,Q}, and {Q,T}. Thus, β and γ can be calculated by the law of cosines.

Additionally, the source position $P_p(x, y)$ for peak point is rewritten as $P_p(x, x \tan \theta_p)$.
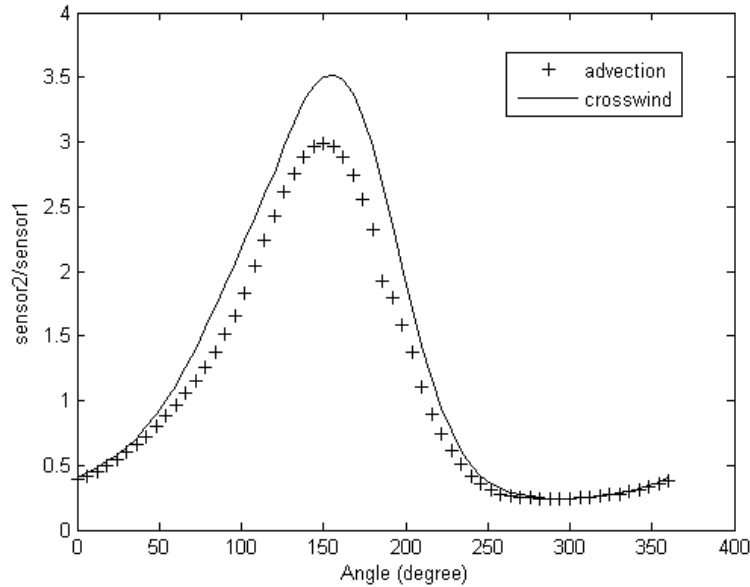
Figure 5. Calculation scheme of peak point angle.

Based on the above analysis, we gathered following information for peak point P_p: (1) Point P_p is on a straight line which is denoted by equation (8); (2) ΔOPQ obey simple triangle geometry. Therefore, a set of equations is established as follows:

$$
\begin{cases}
-\sqrt{\dfrac{1}{1+\tan^2\alpha}} \cdot x + \tan\alpha\sqrt{\dfrac{1}{1+\tan^2\alpha}} \cdot x \tan\theta_p = R \\
Cos(\alpha-\theta_p) = \dfrac{d_{PT}^2 + d_{PO}^2 - d_{OT}^2}{2d_{PT}\cdot d_{PO}}
\end{cases}
\tag{10}
$$

The second equation in equation set (10) is based on the law of cosines. The peak point angle θ_p can be calculated from it. This set of the equations is easily implemented by computer.

Figure 6 shows the curve of the ratio C_2/C_1 for both advection and crosswind situation; obviously they all accord with Gauss distribution and have similar shape. However, they do not reach a peak at the same angle, therefore we can not simply get a fitting equation for C_{2Cross}/C_{1Cross}, since this changes with wind direction. To derive a generic equations for all wind directions, we need to derive an equation for the relation between C_2/C_1 and C_{2Cross}/C_{1Cross}. The differentiating fector between them is the wind direction α which give rise to the peak point angle θ_p. We thus assume that the relation between C_2/C_1 and C_{2Cross}/C_{1Cross} is dependent on the wind direction α and the peak point angle θ_p.
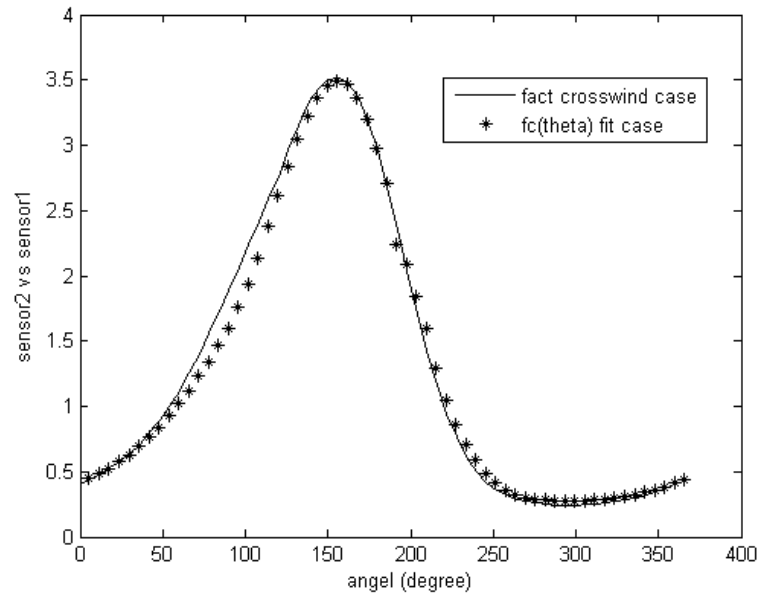
Figure 6. Comparison of C_2 / C_1 for advection and crosswind situation.

We use the Matlab curve fitting toolbox to find an equation relating C_{2Cross} / C_{1Cross} to C_2 / C_1. Let $f(\theta)$ be the function for ratio C_2 / C_1 in advection, then the function $f_c(\theta)$ for C_{2Cross} / C_{1Cross} in crosswind situation has the following relation with direction of crosswind α and peak point angle θ_p based on $f(\theta)$.

$$\frac{C_{2Cross}}{C_{1Cross}} = f_c(\theta) = \frac{1}{\cos \alpha} f(\theta - (\alpha - \theta_p)) \tag{11}$$

Several potential equations were tested; the result shown in Equation (11) was chosen as it had the smallest errors. Figure 7 shows the fitted curve $f_c(\theta)$ against the simulated data C_{2Cross} / C_{1Cross}.

Matlab repots an SSE of 0.1499, R-square of 0.9981, Adjusted R-square of 0.998 and RMSE of 0.05128, which are acceptable.

We explain SSE, R-square, Adjusted R-square and RMSE below [21]:

- SSE -- The sum of squares due to error. This statistic measures the deviation of the responses from the fitted values of the responses. A value closer to 0 indicates a better fit.
- R-square -- The coefficient of multiple determination. This statistic measures how successful the fit is in explaining the variation of the data. A value closer to 1 indicates a better fit.
- Adjusted R-square -- The degree of freedom adjusted R-square. A value closer to 1 indicates a better fit. It is generally the best indicator of the fit quality when additional coefficients are added to the model.
- RMSE -- The root mean squared error. A value closer to 0 indicates a better fit.

From Equation (11), $\theta = f_c^{-1}(\theta)$ allows the direction angle to be calculated.
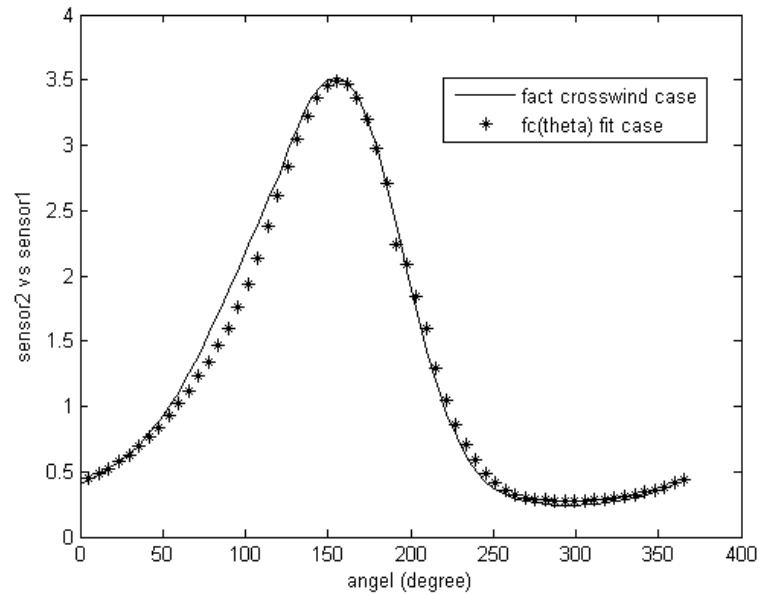
Figure 7. Comparison of fitted curve $f_c(\theta)$ and original C_{2Cross}/C_{1Cross} for crosswind case .

3.3. Breakin the wind case analysis

To deal with the natural wind situations, we must considerthe situation where wind breaks for a period, then recovers as before. This causes some unexpected noise in the signal from the sensors. While the signal decreases, the noise signal will be influenced by a lot of external factors, such as a gentle breeze caused by a passing animal. Usually, the noise does not have a stable pattern. As a result, the break in the wind interferes with the calculation of the source direction.

Figure 8 compares the simulated sensor responses during 5 seconds in no wind break and with wind breaks between 0.7s and 1.4s.

In Figure 8b, the sensor response is interrupted and recovers quickly. By 1.6 seconds it is again stable. We treat the response of the sensors during wind break as noise. A set of new responses is derived by filtering the noise. Using a wind speed sensor, we determine the start and end of a wind break and simply interpolate the response signal during the break, here between 0.8s and 1.5s, and connect the sensor's response at 1.6s to 0.7s. The new sensors' responses in the wind break case are shown in Figure 8c, which is almost the same as the case with on wind break. This simple interpolation technique permits the wind break case to be treated as if it were the wind break free case, by analyzing the steady responses of the sensors. Obviously, the ratio C_2/C_1 will still track the angle, as it works in previous cases.

Based on the approach stated above, the black box inverse problem was successfully solved for a static aroma source.
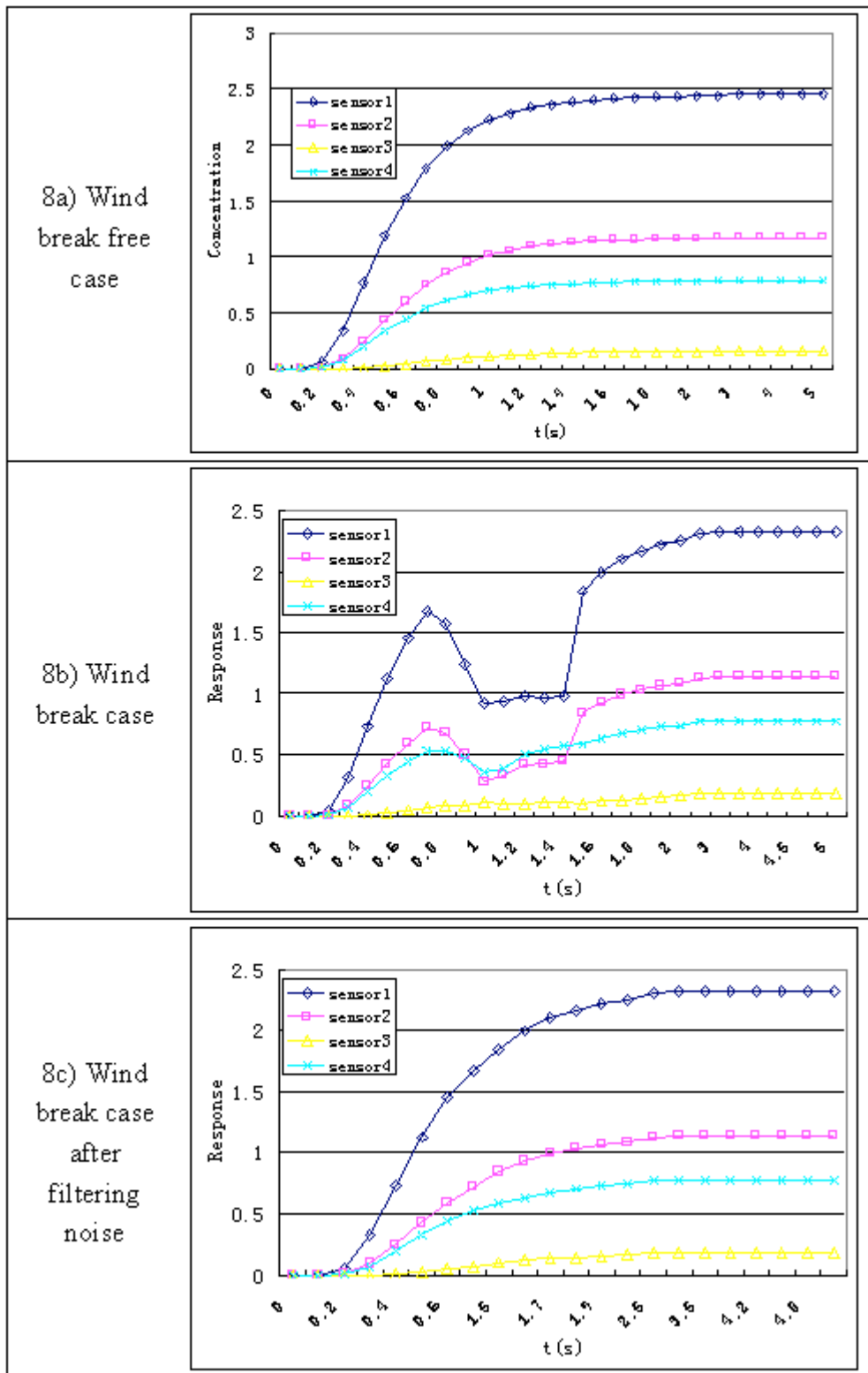
Figure 8. Responses of Sensors for both Wind Break Case and Wind Break Free Case

4. Method for dynamic source detection

Dynamic detection refers to the detection of a source that maybe moving or in some other way varying its output. The basic idea for dynamic source detection is to convert the continuous time into discrete time. We give the marks Φ_i (i=1,2,3,4) to the space separated by the separators for the four

sensors, as shown in Figure 9. The concentration at these four spaces will be changed gradually due to the change of source position. Figure 9 shows the simulated concentration contour for four different source positions in a crosswind with a wind speed of Vx=0.05m/s, Vy=0.03m/s, a diffusion coefficient is $0.03\, m^2/s$, and with the initial source concentration is set to 1000ppm.
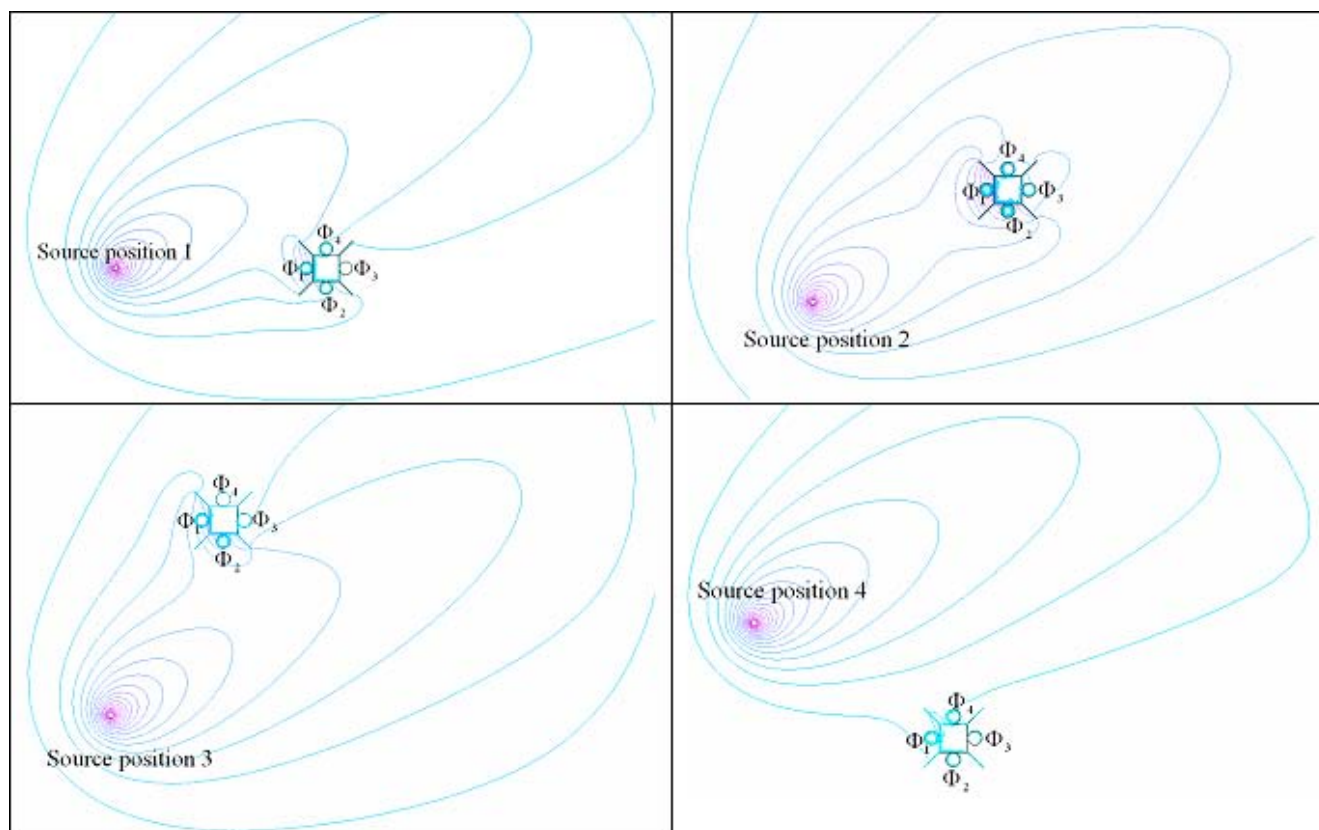
Figure 9. Contour plot of concentration at Φ_i with four different source positions in crosswind case.

As is evident in Figure 9, at the steady situation for different source positions, the concentrations at Φ_i are quite different, and it is time consuming for the concentration to reach the steady values. For example, if the source moves from position 1 to position 2, the concentration at Φ_1 and Φ_2 will change (increase) faster than concentration changes (decreases) at Φ_4. The reason for it is that the diffusion coefficient with a wind blowing is higher than without a wind blowing, and Φ_4 is behind the separator and shielded from the wind. In addition, the concentration distribution is different from the situation observed previously, with a static source at position 2. Since the spatially distributed concentration at position 2 after a movement from position 1 is different from the concentrations around the sensors analysed in section 3, it would appear that we can no longer solve the diffusion PDE as in section 3. As a result, the unstable ratio $C_{2unstable}/C_{1unstable}$ can not be used to determine the source direction. Instead we adopt the approach of digitizing the source movement, approximating it by a series of positions where the source remains for a few seconds to allow the concentration around Φ_i to reach a steady value.

Therefore, we need to quantize time and treat the source movement path as a union of several static points. We assume that the source stays at each position P_i (i is an increasing integer to record the position index for source) for few seconds which allows the ENose system to reach a steady response,

discarding any point at which the sensor responses are not stable. We have a set of simulated concentration for sensor 1 to sensor 4, which can be denoted as C_{ij} (j=1,2,3,4).

We then have a set of ratios, $\Psi_{i2} = \dfrac{C_{i2}}{C_{i1}}$ and $\Psi_{i4} = \dfrac{C_{i4}}{C_{i1}}$. At each source position we have a ratio set $\Lambda_i = \{\Psi_{i2}, \Psi_{i4}\}$. Based on the static solution, we derive the source direction θ_i from Λ_i based on the discussion in section 3.

Consequently, given a known wind speed and direction, the method for dynamic source direction detection will have following scheme:

a) Use the static algorithm to calculate θ_1 for source before movement;

b) Repeat step a) when responses of sensors are stable.

c) Generate θ_i.

After θ_i is calculated, we have an estimate of the direction of movement of the source although this scheme does not record all the details of the source movement.

5. Simulation and results

5.1. Static source case

Simulation is done in both advection and crosswind cases. We set initial concentration of the source to 1000 ppm (source contains only one kind of odor), advection wind speed V_x=5m/s, crosswind wind speed V_x=3m/s, V_y=1.8m/s. The simulation runs for 20 seconds. The purpose of this method is detection of the direction of the source, thus we do not care about the source composition and the type of sensors chosen, but the physical dimensions of the sensors are set to the same as TGS 2610.

Firstly, we set a series of the real source directions at angles of 0^0, 60^0, 120^0, 180^0, 240^0 and 300^0 in the Femlab (finite element analysis) simulation package. We then simulate the steady concentration around sensor 1, sensor 2 and sensor 4 on the conditions stated in the previous paragraph.

Then we use the simulated concentrations as input, based on the equations derived in section 3, to calculate the source direction. The simulated concentrations and calculated source directions are listed in Table 1. The units of C_1, C_2 and C_4 are $\times 10^2$ ppm.

As seen in Table 1, the simulated concentrations for sensors between 120^0 and -120^0 is very small, which in the real world will not cause any responses in the sensors, as the least measurable concentration for FIGARO sensors is between 50ppm to 10ppm [20]. However, in the simulation it is still meaningful to keep four significant figures because the preset initial source concentration is only 1000ppm. As shown in equation (2) when we increase the source initial concentration, the simulated concentration will be increased correspondingly. The increased concentration might be measurable by a real sensor.

The calculated relative error is shown in Table 1. The angle is measured as -180 to +180 relative to the origin instead of 0 to 359 as this makes the relative error calculation more accurate.

The result in Table 1 shows the highest error between 20^0 and 180^0 for both advection and crosswind case, which is because the Gaussian fitting equation has the highest error between 20^0 and 180^0, and curve fitting of equation (11) has the maximum error between 20^0 and 180^0 as well. However, the mean relative error for both advection and crosswind cases are acceptable.

In the real world, we need a wind direction detection sensor to detect the wind direction α to make it an input of the system. If α is smaller than 5^0, the system treats the case as advection case; if α is greater than 5^0, the crosswind case, since wind detection sensors have limited precision. In our simulation, the wind direction is input as a constant.

Table 1. Simulation result and errors for static source.

Real direction		60^0	120^0	180^0	-120^0	-60^0	$360^0(0^0)$	**Mean error**
Advection case	$C_1(\times10^2)$	0. 4082	0. 0054	0. 0005	0. 0054	0. 4082	3. 355	------
	$C_2(\times10^2)$	0. 3938	0. 0132	0. 0012	0. 0023	0. 0995	1. 291	------
	$C_4(\times10^2)$	0. 0995	0. 0023	0. 0012	0. 0132	0. 3938	1. 297	------
	C_2/C_1	0. 9647	2. 444	2. 400	0. 4259	0. 2438	0.3848	------
	C_4/C_1	0. 2438	0. 4259	2. 400	2. 444	0. 9647	0.3866	------
	Measured source direction(θ)	60.71^0	120.54^0	177.41^0	-119.46^0	-59.29^0	$360^0(0^0)$	------
	Relative error	1.17%	0.45%	1.46%	0.45%	1.17%	0.00%	0.78%
Crosswind case	$C_1(\times10^2)$	1. 570	0. 0208	0. 0003	0. 0005	0. 0456	2. 236	------
	$C_2(\times10^2)$	1. 765	0. 0573	0. 0009	0. 0002	0. 0092	0. 9000	------
	$C_4(\times10^2)$	0. 3172	0. 0072	0. 0007	0. 0014	0. 0513	0. 7801	------
	C_2/C_1	1. 124	2. 755	3. 000	0. 4000	0. 2018	0. 4025	------
	C_4/C_1	0. 2020	0. 3462	2. 333	2. 800	1. 125	0. 3489	------
	Measured source direction(θ)	61.46^0	116.38^0	175.01^0	-116.68^0	-62.81^0	360.11^0	------
	Relative error	2.38%	3.11%	2.85%	2.85%	4.47%	0.03%	2.62%

5.2. Dynamic source cases

To simulate the dynamic case we set a source movement path as shown in sketch map, Figure 10. We set 5 points on the path and the source stays at each point for different time segments.

Figure 10 imprecisely describes the following movement: the source stays in position 1 for 20 seconds and then moves to position 2. After staying 1 second in position 2, it moves to position 3 and stays there 10 seconds. Then the source move to position 4 and position 5. It spends 2 seconds in position 4 and stay at position 5 for 40 seconds. The source directions at the 5 positions are 30^0, 45^0, 60^0, 0^0 and -60^0 respectively. We assume that it does not cost time for the source to move from one position to another. Then based on the simulation conditions for the advection case stated in the first

paragraph of this section and making the source move along a circular arch (radius 1.6m) with directions of the 5 positions in Figure 10, we have the following simulation result, shown in Table 2.
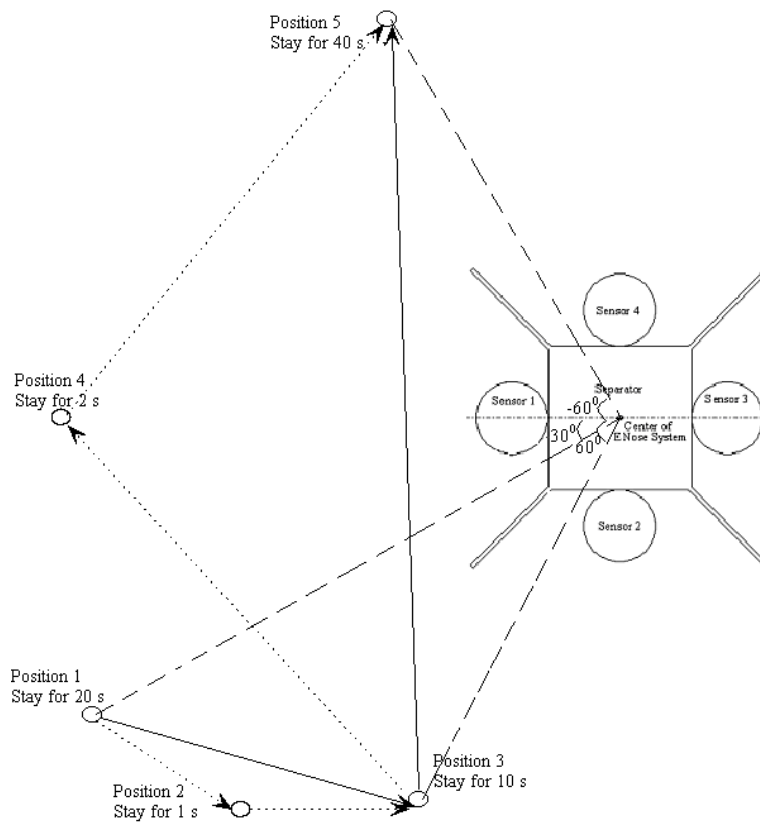
Figure 10. Preset movement sketch map for dynamic source.

The measured source direction for time 21 seconds (position 2) and 33 seconds (position 4) is presented in 2 values, as the calculation results for C_2/C_1 and C_4/C_1 are not corresponding to a same angle.

Table 2. Simulation result and errors for dynamic source tracking.

P	T (s)	C_1 ($\times 10^2$ ppm)	C_2 ($\times 10^2$ ppm)	C_4 ($\times 10^2$ ppm)	C_2/C_1	C_4/C_1	Source direction(θ) measured	real	Relative error
-	0	0	0	0	-	-	-	-	-
1	20	1. 893	1. 128	0. 5367	0. 5959	0. 2835	27.85^0	30^0	7.72%
2	21	1. 6755	1. 007	0. 4514	0.6010	0.2694	28.37^0	45^0	58.62%
							36.14^0		19.69%
3	31	0. 4082	0. 3938	0. 0995	0. 9647	0. 2438	60.71^0	60^0	1.17%
4	33	0. 8548	0. 5971	0. 1210	0. 6985	0. 1416	38.07^0	0^0	100.00%
							null		--
5	73	0. 4082	0. 0995	0. 3938	0. 2438	0. 9647	-59.29^0	-60^0	1.17%

* P represents the position index

* T represents the simulation time

From Table 2, we find that the errors on position 2 and position 4 are very high, which shows the discussion in section 4 is right. The reasonable factors influencing the high errors have already been stated in section 4, which is changed starting concentration distribution and changed diffusion coefficient. As a result, when we dynamically track the source direction, we need to find when the response of the sensors is stable by comparing the concentrations at half second intervals. If the difference between the two values is smaller than 3 ppm, we can consider the response as stable. In our case, positions 1, 3, and 5 are chosen. The readings at position 2 and 4 are discarded due to the high relative errors. The dotted line arrow in Figure 10 presents the unindexed movements; the solid line arrow represents the chosen position and indexed movement. Although the path estimate is abbreviated by using only 3 points it nevertheless shows the correct trend.

Therefore, we get a direction movement scheme, which is shown in Figure 11. The source movement direction scheme gives us a general sense of how the source moves, making it possible to track source directionally.
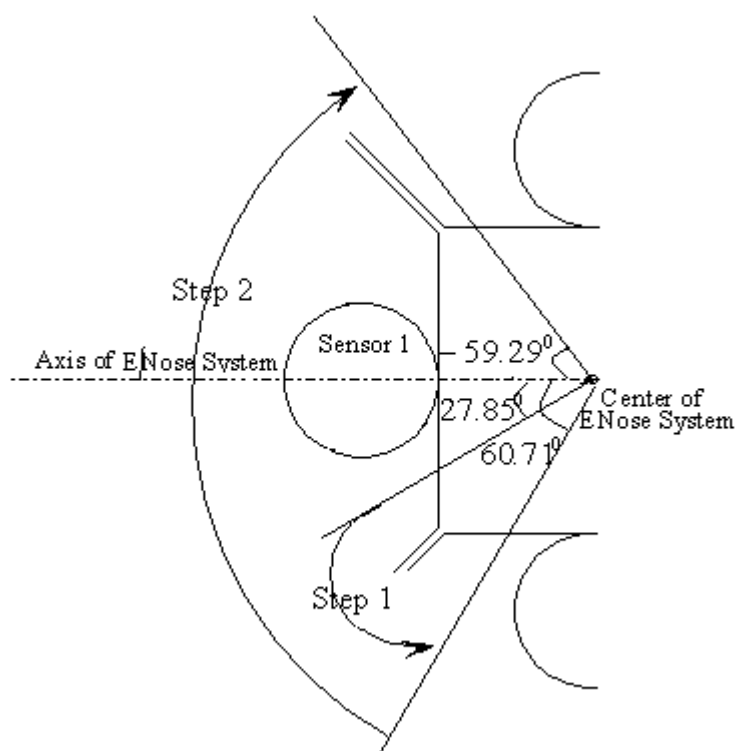
Figure 11. Tracking dynamic source direction.

6. Conclusion and discussion

In this paper, a novel dynamic direction detection method based on a single electronic nose system is presented in natural wind situations by solving a black box inverse problem. The method is successfully established in the advection and crosswind cases, and also for the case of a break in the wind. The simulation results show the accuracy of this method. Also as the calculation is equation based, it is easy to implement and fast to calculate. The direction movement scheme could also be applied to robotic odour tracks, which will work more efficiently than current robotic tracking

systems. The method may be optimized by improving the goodness of fit of the equations for both advection and crosswind cases.

Moreover, the method could be use to locate the odour source, which will make the result more accurate. We could use two of these electronic nose systems to find the cross point of two direction lines, and the cross point will be the source position.

This paper established the theoretical and simulated behaviour of the tracking system. The next step will be to construct and test the hardware. Additionally, locating the source position using a single ENose system is another future research direction for us.

References and Notes

1. Acevedo, F. J.; Maldonado, S.; Dominguez, E.; Narvaez, A.; Lopez, F. Probabilistic support vector machines for multi-class alcohol identification. *Sensors and Actuators B: Chemical* In Press, Corrected Proof.
2. Yu, H.; Wang, J. Discrimination of LongJing green-tea grade by electronic nose. *Sensors and Actuators B: Chemical* In Press, Corrected Proof.
3. Bell, G. A.; Watson, A. J., *Tastes & Aromas, the chemical senses in science and industry*. University of New South Wales Press: Sydney, 1999.
4. Peng, Y.; Min, P.; Yuquan, C.; Guang, L. The recognition of Chinese spirits using electronic nose with dynamic method. *Engineering in Medicine and Biology Society. Proceedings of the 23rd Annual International Conference of the IEEE*, 2001; 2001; pp 3118-3120.
5. Brudzewski, K.; Osowski, S.; Markiewicz, T.; Ulaczyk, J. Classification of gasoline with supplement of bio-products by means of an electronic nose and SVM neural network. *Sensors and Actuators B: Chemical* **2006,** *113* (1), 135-141.
6. Sobanski, T.; Szczurek, A.; Nitsch, K.; Licznerski, B. W.; Radwan, W. Electronic nose applied to automotive fuel qualification . *Sensors and Actuators B: Chemical* **2006,** *116* (1-2), 207-212.
7. Scorsone, E.; Pisanelli, A. M.; Persaud, K. C. Development of an electronic nose for fire detection . *Sensors and Actuators B: Chemical* **2006,** *116* (1-2), 55-61.
8. Ampuero, S.; Bosset, J. O. The electronic nose applied to dairy products: a review . *Sensors and Actuators B: Chemical* **2003,** *94* (1), 1-12.
9. Carmel, L. Electronic nose signal restoration--beyond the dynamic range limit . *Sensors and Actuators B: Chemical* **2005,** *106* (1), 95-100.
10. Carmel, L.; Sever, N.; Lancet, D.; Harel, D. An ENose algorithm for identifying chemicals and determining their concentration . *Sensors and Actuators B: Chemical* **2003,** *93* (1-3), 77-83.
11. Haddad, R.; Carmel, L.; Harel, D. A feature extraction algorithm for multi-peak signals in electronic noses . *Sensors and Actuators B: Chemical* In Press, Corrected Proof.
12. Carmel, L.; Levy, S.; Lancet, D.; Harel, D. A feature extraction method for chemical sensors in electronic noses . *Sensors and Actuators B: Chemical* **2003,** *93* (1-3), 67-76.
13. Padilla, M.; Montoliu, I.; Pardo, A.; Perera, A.; Marco, S. Feature extraction on three way ENose signals. *Sensors and Actuators B: Chemical* **2006,** *116* (1-2), 145-150.

14. Hong, C.; Goubran, R. A.; Mussivand, T. Improving the classification accuracy in electronic noses using multi-dimensional combining (MDC). *Sensors, Proceedings of IEEE*, 2004; 2004; pp 587-590

15. Qin, S. J.; Wu, Z. J. A new approach to analyzing gas mixtures. *Sensors and Actuators B: Chemical* **2001,** *80* (2), 85-88.

16. Loutfi, A.; Coradeschi, S. Relying on an electronic nose for odor localization. *Virtual and Intelligent Measurement Systems. VIMS '02. 2002 IEEE International Symposium on*, 2002; 2002; pp 46-50.

17. Marques, L.; De Almeida, A. T. Electronic nose-based odour source localization. *Advanced Motion Control. Proceedings. 6th International Workshop on,* 2000; 2000; pp 36-40.

18. Jatmiko, W.; Ikemoto, Y.; Matsuno, T.; Fukuda, T.; Sekiyama, K. Distributed odor source localization in dynamic environment. *Sensors, IEEE,* 2005; 2005; p 4 pp.

19. Matthes, J.; Groll, L.; Keller, H. B. Source localization by spatially distributed electronic noses for advection and diffusion. *Signal Processing, IEEE Transactions on [see also Acoustics, Speech, and Signal Processing, IEEE Transactions on]* **2005,** *53* (5), 1711-1719.

20. http://www.figarosensor.com/gaslist.html, September, 28th 2006

21. http://www.mathworks.com/access/helpdesk_r13/help/toolbox/curvefit/ch_fitt9.html, October, 31st 2006